Hindawi
Advances in Meteorology
Volume 2022, Article ID 1409229, 18 pages
https://doi.org/10.1155/2022/1409229

Research Article

Study on the Precursor Signal Capturing of Unfavorable Weather: Months/Years in Advance to Ultra-Early Forecast for Hourly Transient Weather Changes during the Beijing Winter Olympics

Deying Wang,[1] Jizhi Wang ,[1] Yuanqin Yang,[1] Liangke Liu,[2] Wenxing Jia,[1] Junting Zhong,[1] and Yaqiang Wang[1]

[1]*State Key Laboratory of Severe Weather and Key Laboratory of Atmospheric Chemistry of CMA, Chinese Academy of Meteorological Sciences, Beijing 100081, China*
[2]*Department of Earth System Science, Tsinghua University, Beijing 100089, China*

Correspondence should be addressed to Jizhi Wang; jzwang@cma.gov.cn

Received 13 July 2022; Revised 6 September 2022; Accepted 22 September 2022; Published 19 October 2022

Academic Editor: Mojtaba Nedaei

Today, among the existing numerical weather prediction models, those detailing target classifications have been sufficiently explored; however, there are still many weather forecasting goals and needs, and research from theoretical to practical methods still needs additional study. For example, it is important to know as early as possible (months to years in advance) the forecast during a "specific large public event," such as the hourly weather forecast for the Olympic Games. This study elaborates on the theory and methods for such ultra-early prediction of severe transient weather processes in the atmosphere. The main results of this study include (1) establishing the academic concept to capture precursor signals in modern meteorology and provide definitions; (2) establishing methods for capturing precursory signal quantification of unfavorable weather and proposing quantitative measurable thresholds; and (3) proposing the "ultra-early prediction" target task. A typical case is discussed: the meteorological conditions of the Beijing Winter Olympics, which serves as an example of social demand for weather forecasting of "special large-scale public activities," as the case results show that the real-time observations during the Beijing Winter Olympics are consistent with the forecast and followed the precursor signal developed using the theoretical and methodological approaches in this study. The numerical quantization indicators for precursor signals include: (1) for a decrease in the height of the mixed layer hidden in the diurnal change; the precursor signal threshold is defined as a drop of more than 100 m for 3 consecutive days; (2) the signal of the $\delta\Theta e$ displayed as a change by "negative ⟶ positive" of more than seven days in a continuous period. (3) the supersaturation (S) with thresholds reaching 6–7%, as well as the threshold $<0.5\times10^{-3}$ for saturated condensation flux signals (ξ_p); and (4) the hourly resolution transport index of PLAM (parameter linking air-pollution to meteorological condition) PLAM ⟶ obj remaining continuous for 48 h, with its threshold reaching more than 100.

1. Introduction

Currently, although the existing numerical weather prediction models, theories, and practices of weather forecasting classification details have been acceptable, many goals and needs remain, and research on theoretical and practical methods requires additional study. The traditional long-term forecast, the forecast target, is the monthly or annual change trend, and daily or hourly weather changes are regarded as disturbances that need to be smoothly filtered out.

In order to discuss the "detailed target classifications" of forecasts, as shown in Table 1 that the existing traditional forecasting projects for research and operational use (both short-term and long-term forecasts) need to be further technical updated. It is necessary to extend the forecast timeliness but also to increase the refined forecast content,

Table 1: The forecast target classifications of short-medium, long-term term, and climate trends.

	Classifications	Forecasting time limit	Commonly used prediction content	Common predictive keywords
Short-medium term forecast	Now casting	1–6 hours	Strong weather with hourly rate of change	Hourly changes of rain, snow, strong wind and hail
			Rain, snow, strong wind, and hail	Hourly changes of air pollution component
	Short term forecast	24–72 hours	24 hours typhoon and rainstorm	Daily changes of typhoon, cyclone, and rainfall situations
			Visibility and air quality	Daily changes of main air pollution component
	Medium term forecast	5–7 hours	Rainy bands, tropical, or temperate cyclones	Typhoon, cyclone, and rainfall
			The impact of moving	Air quality
Long-term forecast	Monthly forecast	1–3 months	Temperature, humidity, and rainfall	Temperature, humidity, and rainfall
		Or 3–6 months	Drought, floods, and air quality	Monthly forecast and air quality
	Seasonal forecast	Yearly forecast (winter and summer)	Rainy season, dry season, winter, and summer	Rainy season, dry season, winter, and summer
		1-2 years (winter and summer)	The establishment and turning of the monsoon changes	Forecast of the monsoon establishment date
	Yearly forecast	1–5 years	Cold, warm. drought, and flood trends	Cold, warm, drought, and flood trends
Forecast trends in climate	Short-term trends in climate change	5–10 years	Temperature humidity and rainfall	Anomaly corresponds to in 10 years average of temperature humidity and rainfall
	Forecast trends in climate change	>10 years	Ten-year trend of meteorological elements	Anomaly corresponds to in 50 years average of temperature humidity and rainfall
	Ultra-long-term climate predictions	Forecasting trends over a hundred years (century)	Change trends of temperature humidity and rainfall over a century	Anomaly corresponds to a hundred-years average of air temperature

broaden the field of forecasting, and meeting the growth of public demand (see details in Table 1). This study addresses the target of the need for longer forecast timeliness but a more detailed temporal resolution of forecast key content (as given in the red box in Table 1).

However, the concept of ultra-early prediction of atmospheric transient processes is significantly different from previously available forecasting methods. For example, one needs to know as early as possible (months to years in advance) what to expect during "specific large public events," such as hourly schedules of the Olympic Games, hourly schedules for large field trials or exhibition events, etc., which are closely influenced by the weather. Early (e.g., months or years) knowledge from the precursor signal prediction of more granular weather transient processes at an hourly resolution is a new discipline. We define it as "modern ultra-early synoptic meteorology" to distinguish it from long-term prediction and now-casting.

The capture of precursor signals associated with severe transient weather processes in the atmosphere is important for the formation of transient atmospheric processes and their analysis and prediction [1, 2]. In this regard, although it seems to be known that there is a so-called "precursor signal reaction," because it is difficult to capture signals, it is hard to study in depth. Thus, the development of "modern ultra-early synoptic meteorology" has become a recent focus.

With the development and prosperity of human economic and cultural activities in the last few years, there is an urgent need for weather service centers and the public to provide unknown potential changes and possible impacts of unfavorable meteorological conditions in advance for locations where large-scale public activities will occur and provide the necessary time-space weather understanding. For example, climate projections and long-term predictions do not involve transient weather changes of high spatial and temporal resolution. As mentioned above, daily or hourly changes in the weather are regarded as disturbances to be removed. Therefore, the target of "modern ultra-early synoptic meteorology" is to provide the unpredictable impact chain from transient unfavorable meteorological precursor signals to "special large-scale public activities."

The global quadrennial Olympic extravaganza is an atypical large-scale public event. Research on environmental meteorological protection at the 2008 Beijing Summer Olympic Games, which took place successfully in China, has produced numerous results. The U.S. Weather Bulletin reported on the results of the Beijing Olympic Games in China in a long-cover article [3], introducing the multifactor characteristics of atmospheric aerosol pollution and quantifying the results of the impact of adverse meteorological conditions at different stages during the Olympic Games.

With the ultra-early predictions for the February 2022 Winter Olympics in Beijing, the impact of adverse meteorological conditions on air quality has also become a focus of attention for the environmental and atmospheric science

community, and a concern for all relevant Departments of the Meteorological Center and the public.

Although studies have shown that long-term climate change, represented by global warming affecting $PM_{2.5}$, is not dominant, emissions remain the primar,y and endogenous cause of $PM_{2.5}$ in China [4]. The latest research [5] indicated that although the turning points vary in different regions, $PM_{2.5}$ mass concentrations in key regions decreased significantly after 2013 due to clean air actions. In particular, the annual average value of $PM_{2.5}$ in 2020 (including 2021-2022) is nearly the lowest since 1960. This shows that in recent years, China's emission control volume has basically reached a stable standard (especially in winter). However, when emissions are essentially constant (e.g., in winter), the two-way feedback effect of mutual "deterioration" between pollution and unfavorable meteorological conditions also controls the explosive growth of $PM_{2.5}$ in key regions of China [6, 7]. This suggests that it is still necessary to analyze the possible impact of unfavorable meteorological conditions on air quality during the Beijing Winter Olympics.

Environmental meteorological confidence during the Winter Olympics faces many challenges, as exemplified on February 4, 2014, before the Sochi Winter Olympics. Roman Vilfand, the director of the Russian Hydro-meteorological Center, reported that the weather in the Sochi region would be favorable for the competition, with enough snow and a better weather forecast during the week [8]. However, the actual temperature at the Sochi Olympics reached 15°C that year and the Games were seriously affected by unfavorable meteorological conditions. The competition, the men's cross-country snowboarding race, which was scheduled for the afternoon, was also postponed due to heavy fog, originally scheduled for February 16, 19:00 Moscow time, was affected by fog and was postponed until 10:00 on the 17th. Additionally, on the 17th, with no improvement in the weather, several outdoor competitions were postponed due to meteorological conditions. Similarly, at the Vancouver Winter Olympics, temperatures were above average and the Games experienced many adverse meteorological conditions, with the organizers using helicopters to transport snow [8].

It is important to study ultra-early predictions of the possible impact of meteorological conditions on air quality during the Olympics and similar sporting events. International trade in sport has been developing rapidly in recent years, with the Olympic Games in Paris, France in 2024, and China's Chengdu applying to host the 2025 World Games. The technology and research into air quality service guarantees for international sports competitions have become a new focus area for atmospheric science research.

Over the years, China's long-term efforts to reduce air pollution emissions have been remarkably successful. As of 2020, $PM_{2.5}$, SO_2, NOx, and VOCs emissions were reduced by 27%, 20%, 33%, and 24%, respectively, in February compared to a few years earlier. The number of heavy pollution days decreased by 87% from the same period in 2016 [9, 10]. Under the condition of "quasi-zero emission increment," this provides a rare time window to observe the impact of micrometeorological conditions on pollution [11].

This study explores the new development of modern synoptic meteorology and investigates the new method for diagnostic analysis of precursor signals on the impact of emissions and adverse meteorological conditions on air quality during the Winter Olympics in Beijing (Zhangjiakou) for hourly resolution ultra-early prediction weather forecasting.

2. Data and Methods

2.1. Data. This study uses data that includes hourly resolution automatic weather station (AWS) data, ground and high-altitude observation data from the National Information Center, and atmospheric composition station monitoring data [3, 12] to evaluate the spatial and temporal distribution of aerosol pollution in Beijing and Zhangjiakou in February for the past five years. Additionally, it explores the possible influence of meteorological conditions on the Beijing (Zhangjiakou) Winter Olympic Games. The geographical locations of the Winter Olympic Games in Beijing and Zhangjiakou are shown in Figure 1.

To capture precursory hidden signals to introduce as information for establishing ultra-early warnings of "modern synoptic meteorology," an appropriate development approach is to combine both new and traditional methods. In this way, the basic purpose of modern meteorology, the ultra-early warning discipline, as an innovative discipline, is more conducive to being confirmed and understood.

2.2. Capturing and Calculating the Precursor Signals of Height Changes of Atmospheric Pollution Mixing Layer. It has been recognized that the atmospheric boundary layer height is important for diagnosing atmospheric pollution near the ground layer. However, boundary layer information is one of the "hidden signals" that is often difficult to capture.

It is known that while the planetary boundary layer (PBL) parameterization is critical for air quality studies, constrained air quality simulations by PBL parametric schemes are not well quantified under heavy fog pollution boundary layer conditions. Furthermore, the way the boundary layer describes the effects of air pollution is easily copied and confused. For example, the PBL usually refers to the large-scale Ekman dynamic boundary layer. Therefore, it is not reasonable to use the concept of PBL to assess the characteristics of air pollution associated with the near-surface boundary layer. For heavy haze pollution measurement, one of the selected functions of the parameterization scheme is to determine whether the air mass at a specific location meets the wet static stable state of "high humidity" but "rain is difficult to form." Table 2 lists studies of multiple types of boundary layers, including the study of [13].

According to the definition of the wet potential temperature θ_e in (1), when the property in a particular layer (expressed by the P coordinate) of the atmosphere reaches saturation, the saturation mixing ratio is W ($W = W_s$) and Rd/Cp (0.288) is a constant in equation (1).

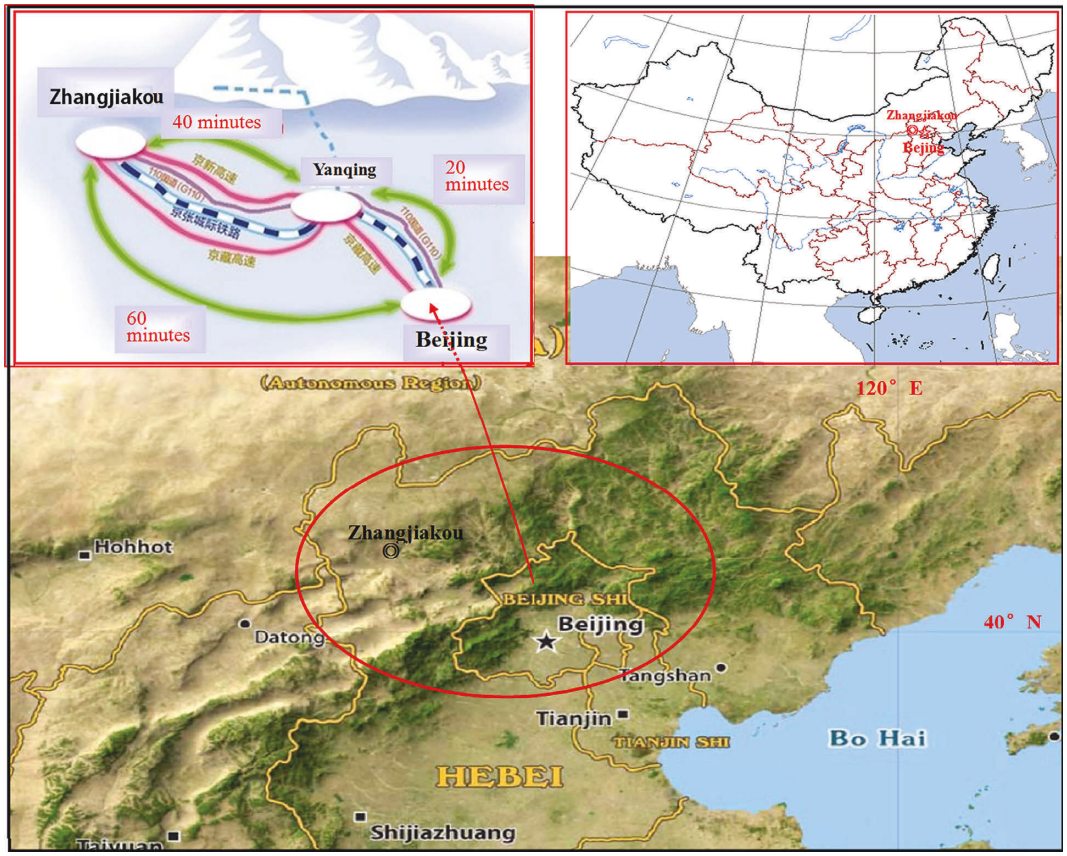

Figure 1: Beijing Winter Olympic Games competition venue in 2022.

Table 2: List of studies on the relationship between air pollutions and boundary layers in recent years.

Abbreviation	Meaning of abbreviations	References
PBL	Planetary boundary layer	[14, 15]
ABL	Atmospheric boundary layer	[16]
SL	Superadiabatic layer	[17]
ML	Mixed layer	[13]
CIL	Capping inversion layer	[16]
CBL	Convective boundary layer	[18]
RML	Residual mixed layer	[19, 20]

Under this height of the particular layer (expressed by P), it is conducive to the continued mixing of pollution when the condensation function fc reaches the critical value of condensation (Note: this is the threshold that needs to be captured), under the condition that the raindrops have not yet been formed. Thus, one of the functions of the air pollution meteorological conditions index is to try to describe whether the local air masses are "stationary" with little variability. θ_e is an important parameter to characterize air mass properties [21, 22]:

$$\theta_e = T\left[\left(\frac{1000}{P}\right)^{Rd/Cp}\right]\exp\left[\left(\frac{Lw_s}{CpT}\right)\right]. \quad (1)$$

The atmospheric processes and structures of the atmospheric mesoscale flow field, condensation, and mechanisms of clouds and precipitation are intrinsically linked. Much has been achieved in these areas of research [12, 23–26] associated with air pollution contributions, as well as the response of emission disturbance changes to meteorological conditions [12, 26].

When the condensation function (f_c) reaches the critical value of condensation but before raindrop formation, the atmosphere is very favorable for the continuation of pollution mixing, particle wetting, and new particle formation acceleration for the continuation of secondary pollution [27, 28]. Then, it is necessary to capture "the threshold" related to humidity. At this atmospheric layer height, the height of the pollution mixing layer (H_PML), one of the defined heights, a precursor signal of air pollution will appear [29]:

$$\text{H\_PML} \approx 6.11 \times 10^2 \times \left(\frac{0.622 + 0.622\left(e_s/p - e_s\right)}{0.622\left(e_s/p - e_s\right)}\right), \quad (2)$$

where e_s is the saturation water vapor pressure. That is what the capturing and calculating for the precursor signal of atmospheric pollution mixing layer height.

2.3. Atmospheric Condensation and Capturing the Precursory Hidden Signal of Supersaturation. The condensation function (also referred to as condensation rate) is expressed as follows:

$$f_c = \frac{f_{cd}}{\left[\left(1 + \left(L/C_p\right)\partial q_s/\partial T\right)_p\right]},$$

$$f_{cd} = \left[\left(\frac{\partial q_s}{\partial P}\right)_T + \gamma_d\left(\frac{\partial q_s}{\partial T}\right)_p\right], \quad (3)$$

$$\gamma_d = \frac{R_d}{C_p}\frac{T}{P},$$

where γ_d is the dry adiabatic lapse rate ($C^\circ m^{-1}$); and C_p, L, q_s, and f_{cd} are the pressure specific heat, latent heat of condensation of water vapor, saturation specific humidity, and dry air condensation rate, respectively. The condensation rate is a function of saturation (S) [29].

Once the atmosphere becomes supersaturated, atmospheric microphysical processes can introduce new observational phenomena and processes into the air. However, research in this area is currently deficient. Supersaturation is the ratio of the mass of the condensed vapor water in the supersaturated state to that in the saturated state, and is a physical quantity expressed as a percentage (%) of the supersaturation [13]:

$$S = \left(\frac{e}{e_s} - 1\right) \times 100\%, \quad (4)$$

where e and e_s are vapor pressure and saturation vapor pressure, respectively. The condensation rate f_c describes some essential characteristics of microphysical processes of aerosols, associated with condensation, atmospheric saturation, clouds, and haze [29]. The reason supersaturated signals are hidden signals that are difficult to capture is that they often occur in the atmosphere, disappear instantaneously, and need to be captured at high resolution (at least hourly). Additionally, when calculating supersaturation (S), it is necessary to introduce that the virtual temperature correction in (4) is Td = Td' (1 + 0.378 ∗ (E/P) [22]. Td is the dew point temperature of the atmosphere.

By (3), when dry air approaches saturation, $_{fcd}$ is close to f_c, and $f_{cd}/f_c \longrightarrow 1$, as follows:

$$\frac{L}{C_{pd}}\left(\frac{\partial q_s}{\partial T}\right)_p \longrightarrow 0. \quad (5)$$

(5) points to a trend in the temperature and humidity field distribution corresponding to a particular critical condensation (f_c), which indicates saturation. Based on this equation, the distributional characteristics of a given temperature trend relative to specific humidity upon reaching saturation point in a uniform pressure field (p = constant on a given isobaric surface) are defined as saturated condensation flux (ξ_p):

$$\xi_p = \frac{L}{C_{pd}}\left(\frac{\partial q_s}{\partial T}\right)_p. \quad (6)$$

According to (6), if (ξ_p) reaches zero or changes little ($<0.5 \times 10^{-3}$) in an actual atmospheric environment, such as within a domain on a given isobaric surface, then this domain is the supersaturated zone that reaches its threshold (ξ_p) and indicates an area with the critical supersaturated precursor signal. The study noted that under the condition of the wetting growth threshold, the humidified particles become haze droplets, but do not continue to grow into raindrops [13, 30, 31].

2.4. Pollution Transport Meteorological Conditions Index ($PLAM_{\longrightarrow obj}$). Most studies have shown that heavy pollution events are closely related to the contribution from surrounding areas. The calculation methods used differ as a result of different transport distance scales. In recent years, some progress has been made in the study of transport methods, such as the study of the backward trajectory path method for long-range transport under the influence of large-scale weather systems [32]. For example, "brown cloud" airflow affecting the Pearl River Delta Region thousands of kilometers away, forming low-visibility pollution weather in mid-March 2008 was traced by backward pathways with pollution emissions that had originated from biomass combustion in the Indo-China Peninsula. Among these, CO, O_3, and PM_{10} concentrations from biomass burning were 2-3 times higher than in other seasons [32]. In the discussion of the backward trajectory, the effect of the wind direction of any surrounding area (observation station) on the projection of the target site was not considered. The early signals captured are significantly uncertain. A series of studies have shown that the PLAM index can be used as a comprehensive pollution-related meteorological indicator to quantify the degree of weather stagnation or stationary ability [3, 4, 7, 11]. Thus, it becomes an indicative index for tracking static and less moving polluted air masses. The advantage of this index is that it can be linearly related to the change in $PM_{2.5}$ mass concentration and is used to measure changes in unfavorable meteorological conditions affecting aerosol pollution in a region (see Figure 2). The index has been successfully used to estimate the quantitative contribution of meteorological factors to the changes in aerosols and optical properties in Beijing during the 2008 Olympics Games [3]. Results of consistently satisfactory applications also include the influence of unfavorable meteorological conditions on changes in aerosol mass concentration and chemical composition from 2006 to 2013 [5].

The originally designed backward trajectory method is a better method that has been widely adopted recently because the original method emphasizes that trajectory tracking needs to be carried out in the process of isoentropic atmosphere, so it can easily track the trajectory of air particles.

Currently common, it is usually based on isobaric surface environment to do trajectory tracking. Therefore, when starting at a certain location, looking backward at the upwind side of the airflow, a certain location is usually selected as the running trajectory of the air. Because the wind vector of the new wind field is transient, it can introduce uncertainty about the tracking results. This study gives a projection of the wind direction of the tracking target taking into account any station of the environment, and the tracking of the trajectory can be more accurate, especially for

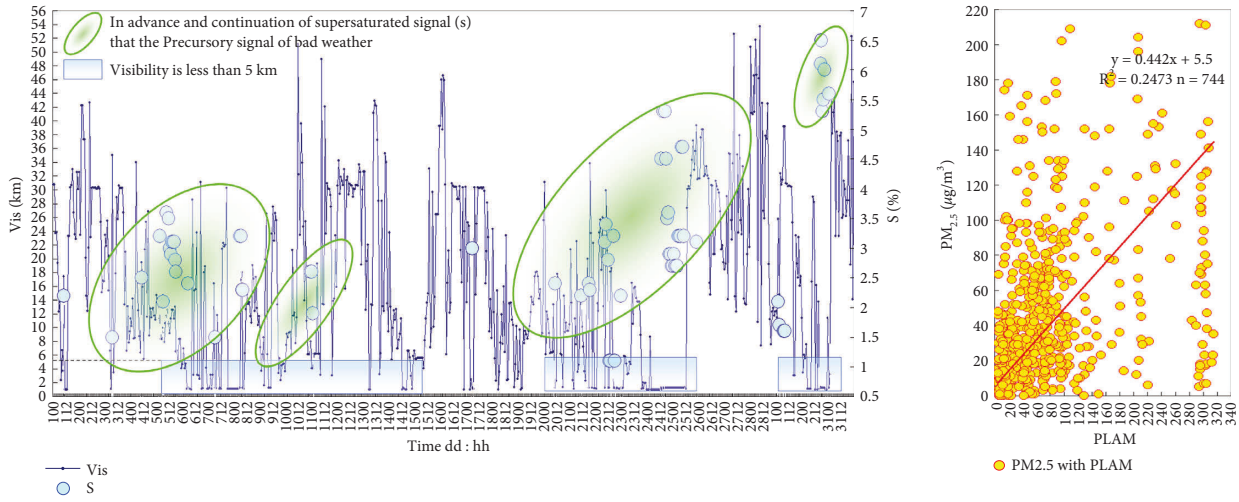

(a) (b)

Figure 2: (a) Hour-by-hour change in visibility and precursor signal supersaturation (S) in February 2022 and (b) correlation analysis between PM2.5 and the PLAM index in February 2022.

the capture of meteorological early signals with large transients, such as the capture of signals under the atmospheric pressure field.

In this study, we discuss the influence of meteorological conditions on the transport of pollutants in the Beijing area using a transport index calculation method for optional "directional targets" (in this study, the site of the Winter Olympics). Equation (7) describes the impact of any area (observatory) on the transport of ambient meteorological conditions, related to its transport distance to the target station, wind speed, and projection of the wind direction to the transmission target:

$$\mathrm{PLAM}_{\longrightarrow \mathrm{obj}} = \mathrm{PLAM}\cos(\alpha - \beta)e^{1/x}, \quad (7)$$

where a and β are the wind direction of the surrounding stations and the angle between the wind direction and the selected target station, respectively, and X is the distance of the surrounding stations relative to the target [33, 34]. The long-distance attenuation of the impact intensity follows an e-exponentially distribution [34, 35].

3. Results and Discussion

3.1. Analysis of Fog–Haze Pollution Characteristics in Beijing (Zhangjiakou) during the Winter Olympic Games in the Past 5 Years

3.1.1. Characteristics of Fog–Haze Pollution Weather in Beijing in February since 2017. The Beijing Winter Olympics Games coincided with the high incidence of the winter fog–haze season in eastern China [6, 36–38]. To explore the observed characteristics of air quality, fog–haze pollution weather, as well as related atmospheric aerosol elements in Beijing in February in recent years, the hourly distributions of visibility and fog–haze pollution in Beijing from February 1 to 28 in 2017 and 2021 are presented in Figures 3(a) and 3(c), respectively. Figures 3(b) and 3(d) show the time series for $PM_{2.5}$, O_3, NO_2, SO_2, PLAM index, and low-layer atmospheric supersaturation (S) in Beijing for February 1–28, 2017 and 2021, respectively. The PLAM index is a parameter linking air quality and meteorological conditions. The higher the value the worse the meteorological conditions, which can be referred in several studies [3, 12]. In accordance with Figure 3, the characteristics of all heavy pollution processes are shown in Table 3. Figure 3 and Table 3 show that four pollution processes occurred in Beijing in February.

2017: from 01:00 on February 3 to 21:00 on February 5, from 19:00 on February 15 to 07:00 on February 17, from 08:00 on February 19 to 07:00 on February 20, and from 05:00 on February 27 to 22:00 on February 28. The four pollution processes in Beijing in February 2017 were mainly characterized by low visibility (VIS), with minimum values of approximately 1 to 2 km. The $PM_{2.5}$, NO_2, O_3, and PLAM index were frequently elevated, with $PM_{2.5}$ reaching a maximum of 351 $\mu g/m^3$, NO_2 reaching 169 $\mu g/m^3$, and O_3 reaching 102 $\mu g/m^3$. Two pollution processes showed an atmospheric supersaturation, with the supersaturation (S) higher than 3.2%. In February 2021, there were also two heavy pollution processes in Beijing, which occurred from 06:00 on February 11 to 15 and from 06:00 on February 26 to 00:00 on February 28. Their main characteristics indicated low VIS with a VIS <1.1 km. Similarly, the $PM_{2.5}$, NO_2, O_3, and PLAM index were frequently elevated, with $PM_{2.5}$ reaching 472 $\mu g/m^3$, NO_2 reaching 102 $\mu g/m^3$, and O_3 reaching 117 $\mu g/m^3$. Atmospheric supersaturation occurred in some processes, exceeding 5.7%.

3.1.2. Characteristics of Fog–Haze Pollution Weather in Zhangjiakou in February since 2017. The hourly distributions of VIS and fog–haze pollution in Zhangjiakou in February 2017 and February 2021 are presented in Figures 4(a) and 4(c), respectively. Figures 4(b) and 4(d) show the time series of $PM_{2.5}$, O_3, NO_2, SO_2, PLAM index,

FIGURE 3: Hourly distributions of visibility (VIS) and fog–haze in Beijing for February 1–28, 2017 (a) and (c) 2021; hourly observed distributions of $PM_{2.5}$, O_3, NO_2, SO_2, the PLAM index, and low-layer atmospheric supersaturation (S) for February 1–28, (b) 2017 and (d) 2021.

and low-level atmospheric supersaturation(s) in Zhangjiakou in February 2017 and February 2021, respectively.

As shown in Figure 4 and Table 4, four pollution processes occurred in Zhangjiakou in February 2017, which belong to the same pollution processes as the four pollution processes in Beijing during the same period. In 2017, the four pollution processes were mainly characterized by low VIS, with minimum values of less than 1.1 km. Elevated values for $PM_{2.5}$, NO_2, O_3, and PLAM index were common, and SO_2 reached 245 $\mu g/m^3$. Some processes had atmospheric supersaturation exceeding 4.2%. In 2021, two heavy pollution processes were also primarily characterized by low VIS. Meanwhile, NO_2 reached 102 $\mu g/m^3$ and O_3 reached 117 $\mu g/m^3$. Some processes were characterized by atmospheric supersaturation, with supersaturation (S) higher than 4.6%.

The above analysis shows that in 2017 and 2021, the pollution process timeframe was synchronized in Zhangjiakou and Beijing. The process lasted a long time, with the longest haze pollution process reaching four days (from February 11 to 14) in 2021. In February 2017, $PM_{2.5}$ peaked at 472 $\mu g/m^3$ in Beijing, while SO_2 peaked at 245 $\mu g/m^3$ in Zhangjiakou.

Table 5 presents the statistical analysis of the impact of meteorological conditions on air quality for every five-day period in February during the same period of the Beijing Winter Olympics over the past five years (2017 to 2021). From the air quality situation (per 5 days) in February for the last 5 years, the Winter Olympics were more prone to unfavorable meteorological conditions during the same period, which needs more attention in order to improve the fine monitoring and early warning capabilities. Research on meteorological protection for large competitive sports, weather impact "precursor signal" and warning techniques are very important.

Table 3: Weather phenomena and atmospheric aerosol elements of the pollution process in Beijing for February 2017 and 2021.

Pollution processes in Beijing for Feb 2017	Visibility	Weather: haze
① 01:00 3 Feb to 21:00 05 Feb	① Vis_mini. = 1.0 km	√
② 19:00 15 Feb to 07:00 17 Feb	② Vis_mini. = 1.1 km	√
③ 08:00 19 Feb to 07:00 20 Feb	③ Vis_mini. = 2.2 km	√
④ 05:00 27 Feb to 22:00 28 Feb	④ Vis_mini. = 2.1 km	√
Pollution processes in Beijing for Feb 2017	Factor of aerosols and PLAM	
① 18:00 04 Feb to 22:00 04 Feb	① $PM_{2.5} = 351\ \mu g/m^3$ $NO_2 = 169\ \mu g/m^3$, O_3↑$102\ \mu g/m^3$ PLAM = 182	
② 07:00 15 Feb to 19:00 16 Feb	② $PM_{2.5} = 275\ \mu g/m^3$ PLAM = 183, $S = 3.2\%$	
③ 13:00 20 Feb to 00:00 23 Feb	③ $PM_{2.5} = 176\ \mu g/m^3$ PLAM = 190, $S = 3.2\%$	
④ 05:00 27 Feb to 22:00 28 Feb	④ $PM_{2.5} = 98\ \mu g/m^3$ $O_3 = 97\ \mu g/m^3$ $NO_2 = 121\ \mu g/m^3$	
Pollution processes in Beijing for Feb 2021	Visibility	Weather: haze
① 06:00 11 Feb to 19:00 15 Feb	① Vis_mini. = 1.3 km	√
② 06:00 26 Feb to 00:00 28 Feb	② Vis_mini. = 1.1 km	√
Pollution processes in Beijing for Feb 2021	Factor of aerosols and PLAM	
① 06:00 11 Feb to 19:00 15 Feb	① $PM_{2.5} = 472\ \mu g/m^3$ $NO_2 = 106\ \mu g/m^3$, O_3↑$117\ \mu g/m^3$ PLAM = 190	
② 06:00 26 Feb to 00:00 28 Feb	② $PM_{2.5} = 198\ \mu g/m^3$ PLAM = 185, $S = 5.7\%$ $O_3 = 113\ \mu g/m^3$	

Table 5 shows the statistical projections of the contribution to the predicted impact of meteorological conditions every 5 days of the 2022 Winter Olympics in Beijing, based on the information for day-by-day and hour-by-hour, during the same period of the 2017–2021 Winter Olympics, (good weather: expressed in light blue, its probability (%) expressed in numbers as well as the area of the blue box in the table; adverse weather: expressed in brown, its probability (%) expressed in numbers as well as the area of the brown box in the table).

3.2. Unfavorable Microscale Meteorological "Precursor Signals" of Historical High-Frequency Fog–Haze Pollution during the Same Period of the Beijing Winter Olympics

3.2.1. Precursor Signals Response of Pollution Mixing Layer Height to Fog–Haze in Beijing. To explore the influence of meteorological conditions on the fog–haze pollution during the historical period of the Beijing Winter Olympic Games, the distribution of the PLAM index and the height of the pollution mixing layer were calculated using hourly resolution meteorological parameter observation information, which shown in Figure 5. It can be seen that:

(1) As shown in Figures 5(a) and 5(b), a continuous decrease in the H_PML was observed 5–7 days before the two severe fog–haze processes in Beijing (from 06:00 on February 11 to 19:00 on February 15, and from 06:00 on February 26 to 28) (dashed arrows in Figure 5(b)). Along with the continuous decrease in H_PML, an increase in the PLAM index was observed (shown in the boxed area in Figure 5(a)). With the PLAM rising from less than 40 on February 10 to 200 on February 12, and from less than 40 on February 25 to more than 180 on February 28 (shown in the yellow boxed area in Figure 5), the events corresponded to two heavy fog–haze processes on February 15 and 28.A continuous gradual decrease in H_PML was observed 5–7 days before the two severe fog–haze processes, indicating that the change in H_PML has a significant precursor signal indication. The fact that this change in H_PML is a precursor signal of fog–haze has been observed throughout China [39].

(2) From Figure 5(c), we can see that wet potential temperature (Θ_e) is an important physical quantity indicating the property characteristics of air masses [21]. It provides a foundation for prevention and warning against polluted weather. The precursor signal response of at least 5–7 days is of considerable importance for air quality forecasts during the Beijing Winter Olympics.

As shown in Figure 5(b), each period of heavy pollution (shown in the heavy yellow box area in Figure 5(b)) is accompanied by the process of less change in $\delta\Theta_e$ ($\delta\Theta_e \longrightarrow 0$) and the successive increase in $\delta\Theta_e$ (↑), generally also 7–10 days in advance. Thus, the change in the static stability in the lower atmosphere to mixed control of warm air masses indicated by temperature and humidity is a precursor signal of heavy fog–haze pollution in Beijing. As can also be seen in Figure 5(c), the less variable and successive elevation process

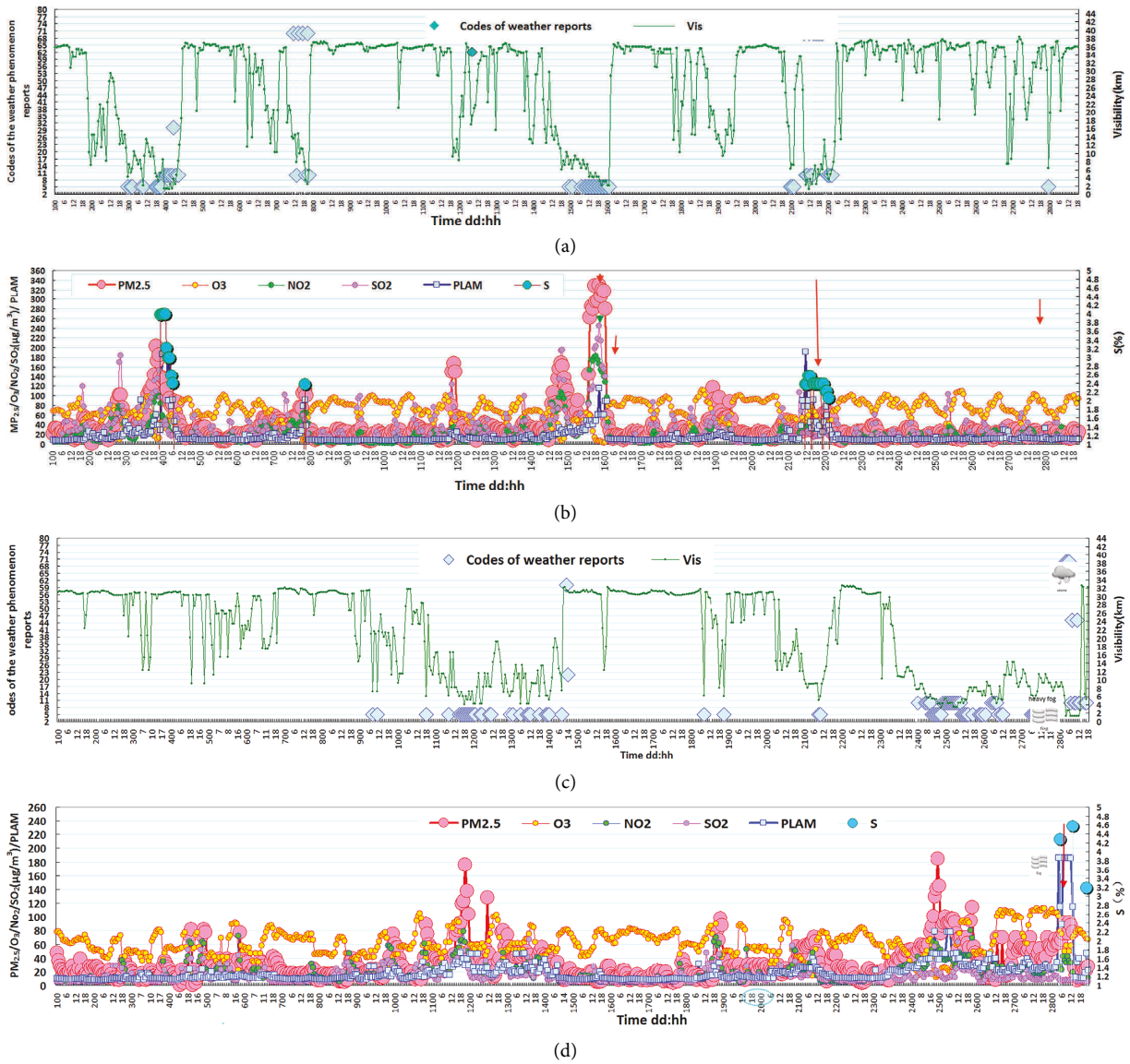

FIGURE 4: Hourly distributions of visibility and fog–haze pollution in Zhangjiakou for February 1–28, (a) 2017 and (c) 2021; hourly observed distributions of $PM_{2.5}$, O_3, NO_2, SO_2, the PLAM index, and low-level atmospheric supersaturation(S) for February 1–28, (b) 2017 and (d) 2021.

of $\delta\Theta_e$ 7–10 days in advance, the supersaturation (S) spikes significantly, from 3.5% to 6–7% (shown by the light blue bubble in Figure 5(c)).

3.2.2. Application Test of Early Capture of Supersaturation Precursor Signal Potential Aerosol Pollution Zone. In order to discuss the universality of early capture precursor signals in areas where contamination may occur, Figure 6 presents several typical cases of significant pollution in history. The abovementioned examples, namely, characteristics of the precursor signals ξ_p and supersaturation (S) calculated by (5) and (6), respectively, for the period from July 24 to 27, 2008 during the 2008 Beijing Olympic Games and the case during July 19 to 22 of 2018 (Figure 6). Table 6 presents typical cases like the Beijing Olympics during 2008, including Vancouver, Canada (where the Winter Olympics have been held), and New York, USA.

To discuss the universality of the microphysical condensation process of pollution precursor signals on seasonal and regional diagnostics, here, are examples of summer pollution. The case of Vancouver indicated that during the heat wave weather from 29 July to 2 August, in broad areas of British Columbia, including Vancouver, $PM_{2.5}$ increased from less than 6 $\mu g/m^3$ to 16 $\mu g/m^3$. The case of New York indicated that the rising aerosol density (SO_4_f) peaked at 120 $\mu g/m^3$in New York during the period from 1 July to 31 August 2006.

From Figure 6(a), at 20:00 on July 16, 2018, 48 h before the peak of $PM_{2.5}$ in Beijing, the supersaturation was 4%, and it continued to grow hourly, and by the 18th, it increased to 22%. Supersaturation of 4% within the 24 h before the peak at 00:00 on July 20, also, increased hourly, reaching 20%.

Table 4: Weather phenomena and atmospheric aerosol elements of the pollution process in Zhangjiakou for February 2017 and February 2021.

Pollution processes in ZJK for Feb 2017	Visibility	Weather: haze
① 19:00 03 Feb to 00:00 04 Feb	① Vis_mini. = 1.3 km	√
② 00:00 15 Feb to 00:00 16 Feb	② Vis_mini. = 2.1 km	√
③ 00:00 21 Feb to 00:00 22 Feb	③ Vis_mini. = 1.2 km	√
④ 00:00 27 Feb to 00:00 28 Feb	④ Vis_mini. = 6.3 km	√
Pollution processes in ZJK for Feb 2017	Factor of aerosols and PLAM	
① 20:00 02 Feb to 12:00 04 Feb	① PLAM = 193 $PM_{2.5}$ = 203 μg/m^3 SO_2 = 184 μg/m3	S = 4.0%
② 07:00 15 Feb to 19:00 16 Feb	② $PM_{2.5}$ = 168 μg/m^3 SO_2 = 245 μg/m^3	NO_2 = 182 μg/m^3
③ 00:00 21 Feb to 08:00 22 Feb	③ $PM_{2.5}$ = 168 μg/m^3 PLAM = 191, S = 2.6%	SO_2 = 107 μg/m^3
④ 17:00 25 Feb to 17:00 27 Feb	④ O_3 = 109 μg/m^3 SO_2 = 103 μg/m^3	
Pollution processes in ZJK for Feb 2021	Visibility	Weather: Haze
① 06:00 11 Feb to 19:00 15 Feb	① Vis_mini. = 1.3 km	√
② 06:00 26 Feb to 00:00 28 Feb	② Vis_mini. = 1.1 km	√
Pollution processes in ZJK for Feb 2021	Factor of aerosols and PLAM	
① 06:00 11 Feb to 19:00 15 Feb	① $PM_{2.5}$ = 472 μg/m^3 NO_2 = 106 μg/m^3, $O_{3\uparrow}$ PLAM = 190	117 μg/m^3
② 06:00 26 Feb to 00:00 28 Feb	② $PM_{2.5}$ = 198 μg/m^3 PLAM = 185, S = 5.7% O_3 = 113 μg/m^3	

Table 5: Statistical analysis of the impact of meteorological conditions on air quality every 5 days during the same period of the Beijing for the years 2017 to 2021.

Year	Date	1 to 5	6 to 10	11 to 15	16 to 20	21 to 25	26 to 29
2017	Visibility	3.1 km	3.3 km	2.1 km	2.2 km	3.3 km	2.2 km
	Weather phenomenon	Haze	Haze	Haze	Haze	Haze	Haze
	PLAM	182	79	183	115	190	115
	$PM_{2.5}$	351	114	275	176	141	98
2018	Visibility	6.2 km	4.2 km	25.9	2.3 km	30.2 km	3.2 k
	Weather phenomenon		Haze		Haze		Haze
	PLAM	32	32	47	187	47	185
	$PM_{2.5}$	51	99	79	250	64	227
2019	Visibility	1.2 km	30.4 km	1.1 km	1.3 km	1.2 km	3.2 km
	Weather phenomenon	Haze	Clear	Haze	Haze	Haze	Haze
	PLAM	189	9.3	190	188	193	90
	$PM_{2.5}$	278	61	88	37	259	114
2020	Visibility	2.4 km	11 km	1.2 km	33.9 km	1.2 km	1.3 km
	Weather phenomenon	Haze	Haze	Haze	Clear	Haze	Haze
	PLAM	89	189	183	12	186	186
	$PM_{2.5}$	59	193	268	32	146	161
2021	Visibility	14.6 km	5.6 km	1.3 km	30.5 km	31.2 km	9.4 km
	Weather phenomenon	Clear	Haze	Haze	Clear	Clear	Haze
	PLAM	10	18	190	11	13	185
	$PM_{2.5}$	56	124	472	38	80	198 μg/m^3
Contribution (%)	Fine (baby blue) Weather (%)	56%	44%	20%	50%	40%	12%
	Unfavorable Meteorological conditions (%) (brown)	44%	56%	80%	50%	60%	84%

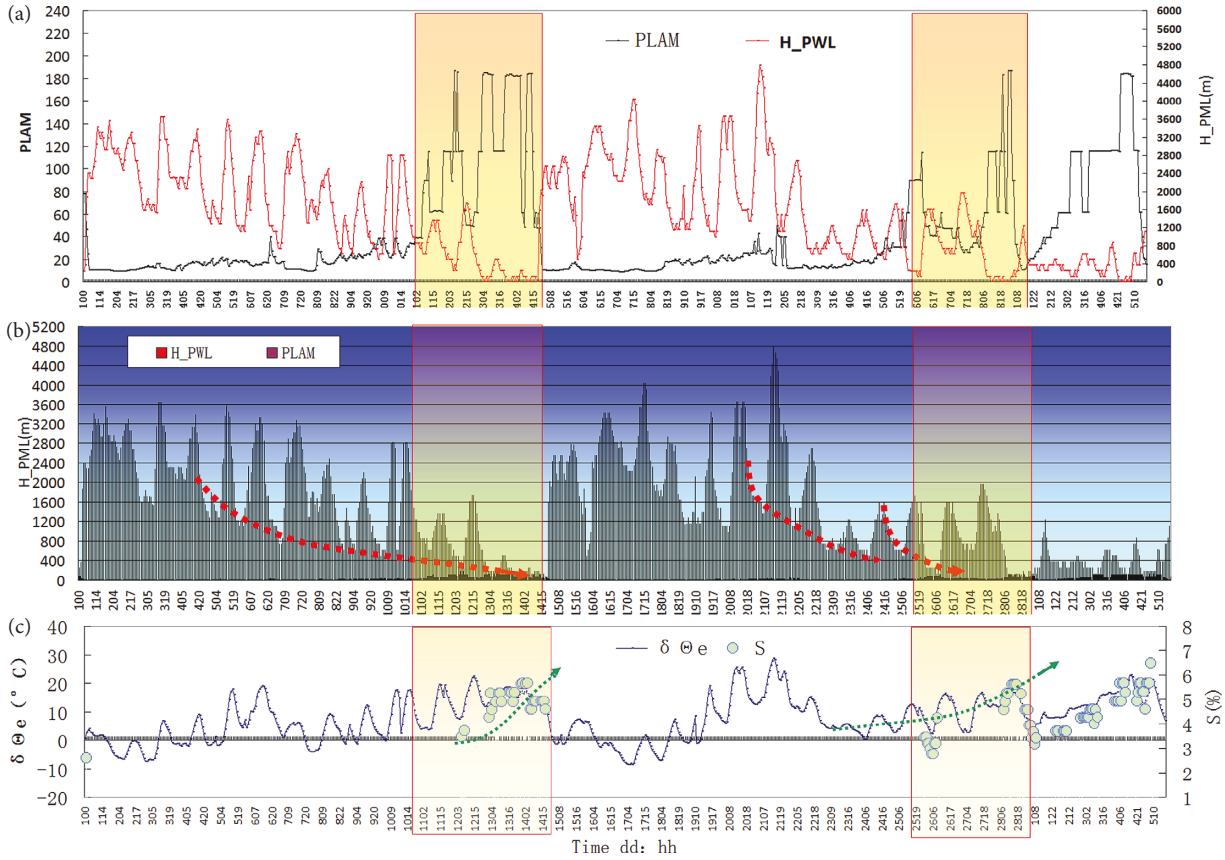

FIGURE 5: (a) Hourly distribution of PLAM index and height of mixing layer (H_PML) in Beijing in February 2021, (b) distribution of perturbed daily oscillation variation minimum of H_PML and (c) hourly wet potential temperature variation ($\delta\Theta e$) and the distribution of atmospheric supersaturation (S).

Table 6 shows the precursor signals (ξ_p) in Beijing, Vancouver, and New York. It is shown to have consistent results ($<0.5\times10^{-3}$) in summer, winter, and transitional spring cases. This suggests that "supersaturation under condensation rate threshold conditions" in the atmosphere may result in a high density of accumulated aerosols. This finding is almost virtually universal and applies across the North Hemisphere. So that the precursor signals of supersaturation can be widely used in the Northern Hemisphere for the identification, diagnosis, and prognosis of potential aerosol pollution.

3.2.3. Precursor Signal Characteristics of Pollution Transport by Calculating the Transport Index ($PLAM_{\longrightarrow obj}$) from the Surrounding Pollution Area. Figure 7(a) shows the pollution transport at 00:00 on February 27, 2021, calculated by (7), with the contributions by the index of pollution meteorological conditions oriented towards Beijing (PLAM ⟶ obj).

The directional transport of surrounding pollutants to Beijing under the influence of meteorological conditions is used to analyze the precursor signal quantitative response of the $PLAM_{\longrightarrow obj}$ index before the pollution event in Beijing at 15:00 on February 28, 2021 (corresponds to the heavy pollution incident in Beijing on February 28 (see Figure 7(a))). Figures 7(c) and 7(d) are the same as Figure 7(a), calculated for 00:00 on February 11 and 12, 2021, respectively, to obtain the response of the precursor signal of the $PLAM_{\longrightarrow obj}$ index before the peak of 472 $\mu g/m^3$ at 09:00 on February 13, 2021. As can be seen from Figure 7, the quantitative $PLAM_{\longrightarrow obj}$ index 39 h before the pollution in Beijing at 15:00 on February 28, 2021 (see Figure 3(d), $PM_{2.5}$ concentration reached 188 $\mu g/m^3$) indicates that there was positive transport from the eastern Shandong Peninsula with the value of 50–100. The values of the hourly resolution $PLAM_{\longrightarrow obj}$ index provide information on the transport of pollution prior to the precursor signal response in Beijing.

The ground weather map in Figure 7(b) at 06:00 on February 27, 2021, in line with the direction of the high pollution transport belt, is a partial easterly airflow. Another warm and humid airflow south of the subtropical high pressure is a large-scale airflow system for pollution in Beijing. The ground weather map showed that the Beijing–Tianjin–Hebei region, Shandong, and Shanxi–Henan also demonstrated fog–haze weather on a large-scale. Similarly, with the Beijing Winter Olympic Games at the same time of 09:00 on February 13, 2021, a peak of up to 472 $\mu g/m^3$, a record heavy pollution event, respectively, 57 h and 39 h in advance, that is, 00:00 on February 11 and 12 (Figures 7(c) and 7(d)). It has been quantitatively established (the value up to 100) that positive values are

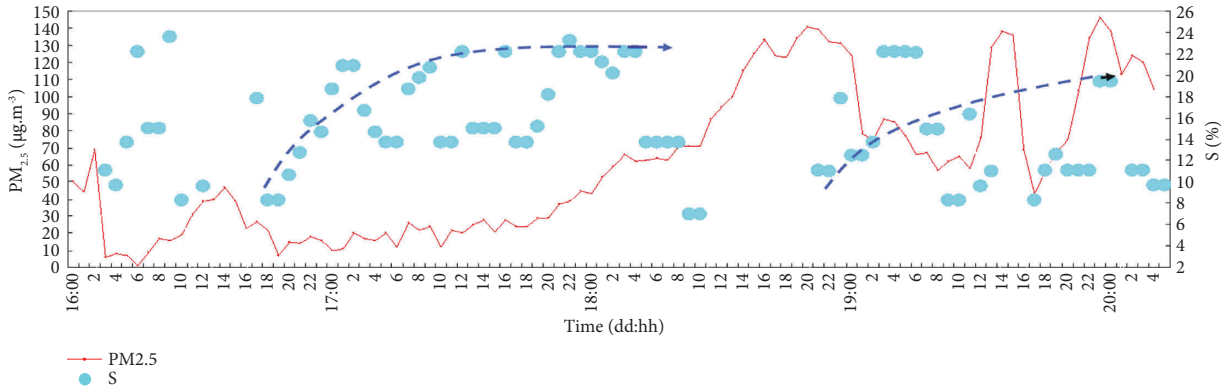

(a)

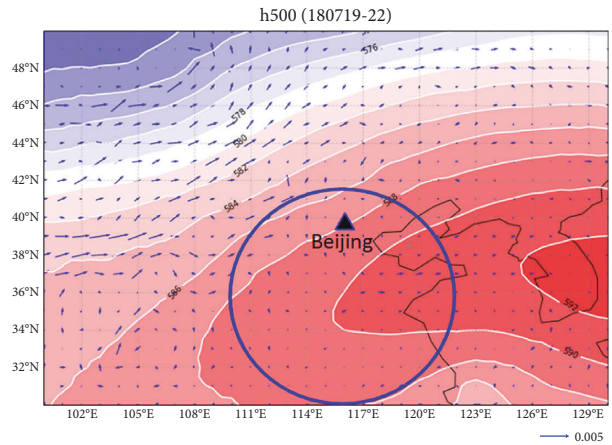

(b)

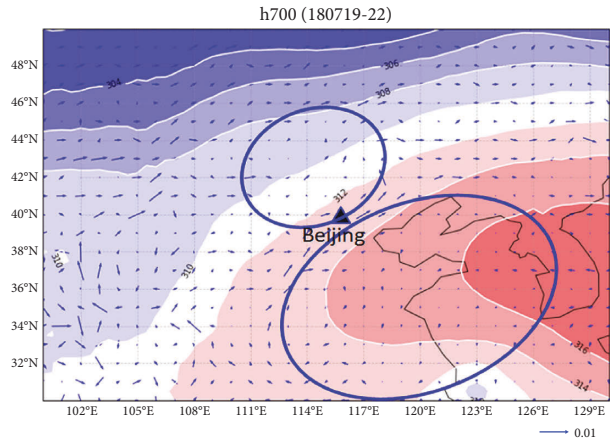

(c)

Figure 6: Continued.

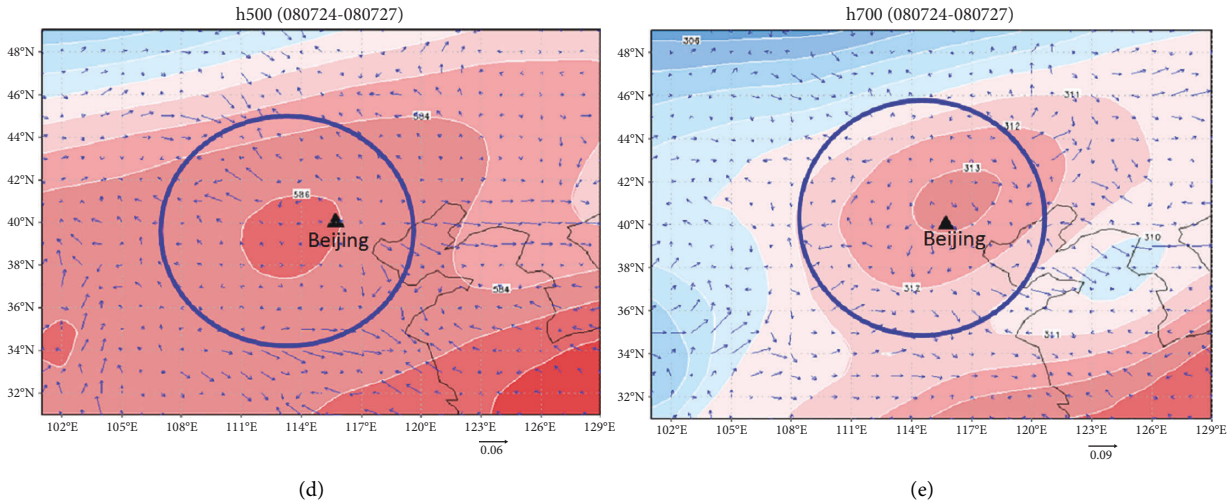

Figure 6: (a) Hourly distributions of $PM_{2.5}$ and atmospheric supersaturation (S) in 16–20 July 2018; (b) geo-potential heights (white line: gm) and saturated condensation flux (ξ_p) at 500 hPa of isobaric surfaces in the pollution process in 19–22 July 2018, (c) the same as (b) but for 700 hPa, (d) the early period of 2008 Beijing Summer Olympic Games in 24–27 July 2008 for 500 hPa, (e) the same as (d), but for 700 hPa; Scales of arrows are 0.005, 0.01, 0.06 and 0.09×10^{-3},respectively.

Table 6: Saturated condensation flux (ξ_p) and geo-potential heights at various isobaric surfaces over Beijing, Vancouver, and New York.

Isobaric surface (hPa)	Beijing		Vancouver		New York	
	Geo-potential height	ξ_p ratio* $\times 10^{-3}$	Geo-potential height	ξ_p ratio $\times 10^{-3}$	Geo-potential height	ξ_p ratio
300	968	0.19	968	0.39	—	—
500	584	0.43	586	0.31	584	0.44
700	314	0.48	316	0.75	—	—
850	158	0.48	148	0.47	154	0.35

*ξ_p ratio refers to the ratio of mean value of ξ_p center of its surrounding area.

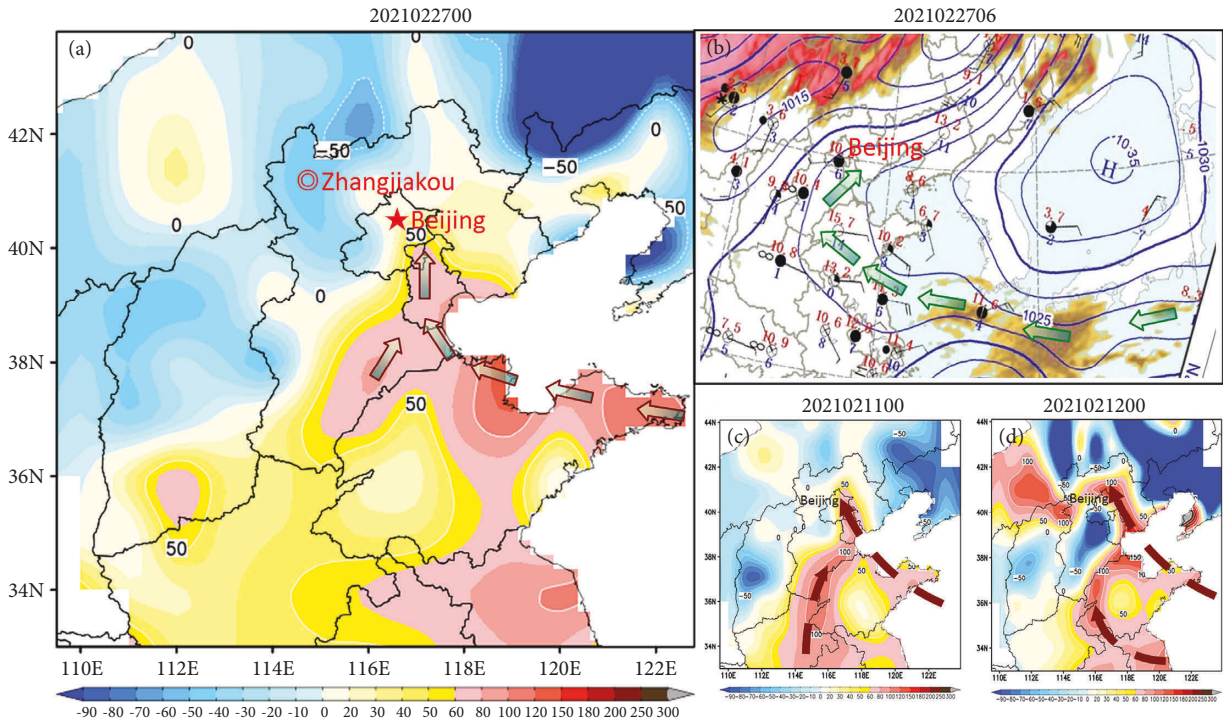

Figure 7: (a) Directed transport of pollution meteorological conditions index ($PLAM_{\rightarrow obj}$) to Beijing at 00:00 on February 27, 2021, (b) surface weather map of Beijing–Tianjin–Hebei region at 06:00 on February 27, 2021, (c) directed transport of pollution meteorological conditions index ($PLAM_{\rightarrow obj}$) to Beijing at 00:00 on February 11, 2021, and (d) directed transport of pollution meteorological conditions index ($PLAM_{\rightarrow obj}$) to Beijing at 00:00 on February 12, 2021.

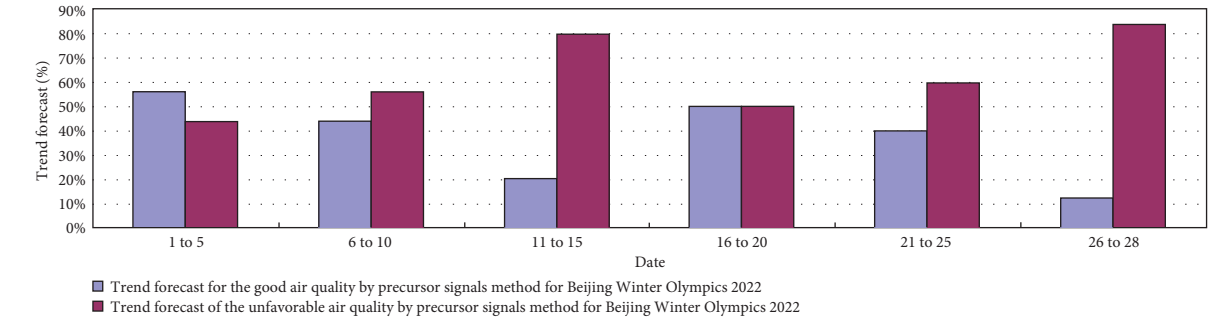

(a)

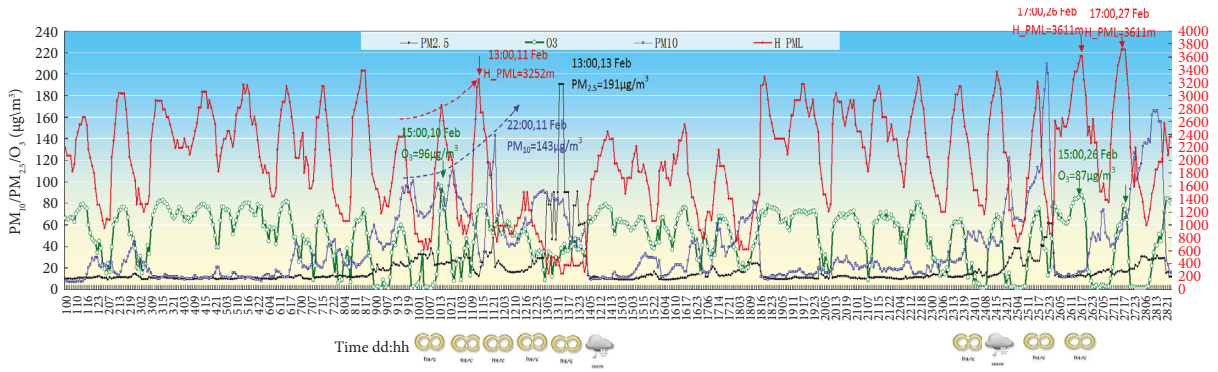

(b)

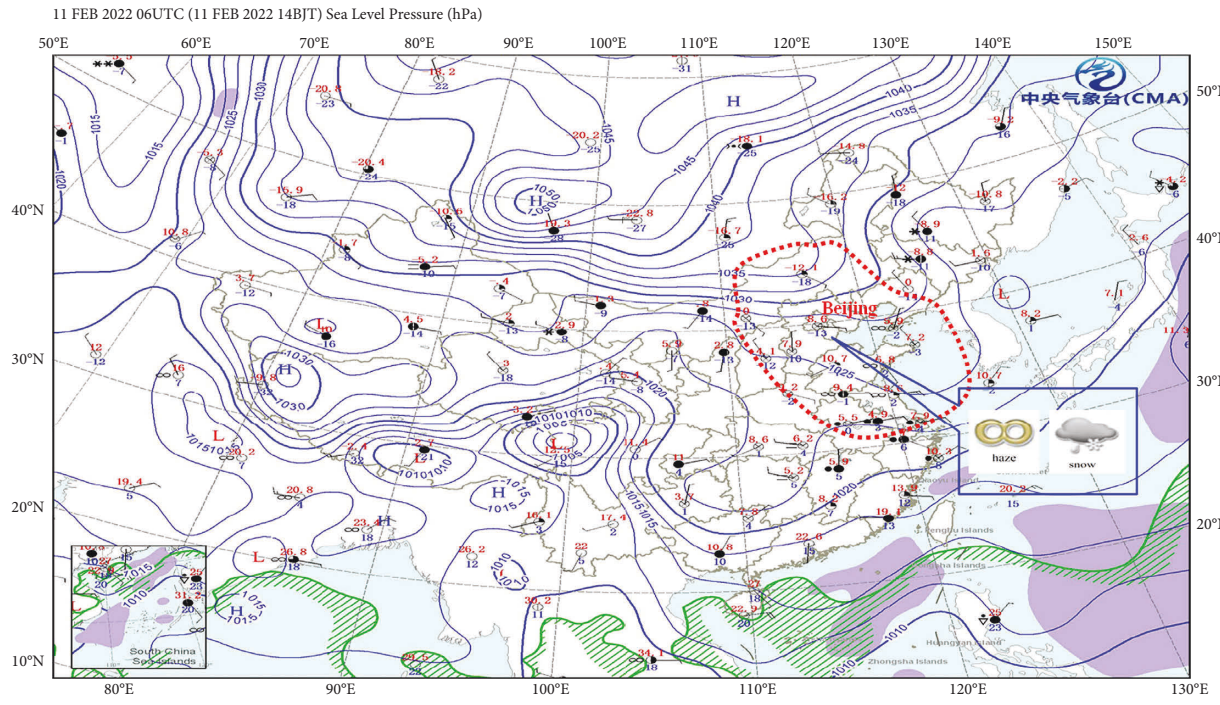

(c)

Figure 8: (a) Forecast analysis of the impact of meteorological conditions on air quality in the same period as the Beijing Winter Games for the past five years (2017 to 2021) based on the data of Table 5; (b) the high-resolution (hourly) weather changes with observations for the period of Beijing Winter Olympics (February 2022); (c) a map of the ground weather at 14:00 on February 11, 2022.

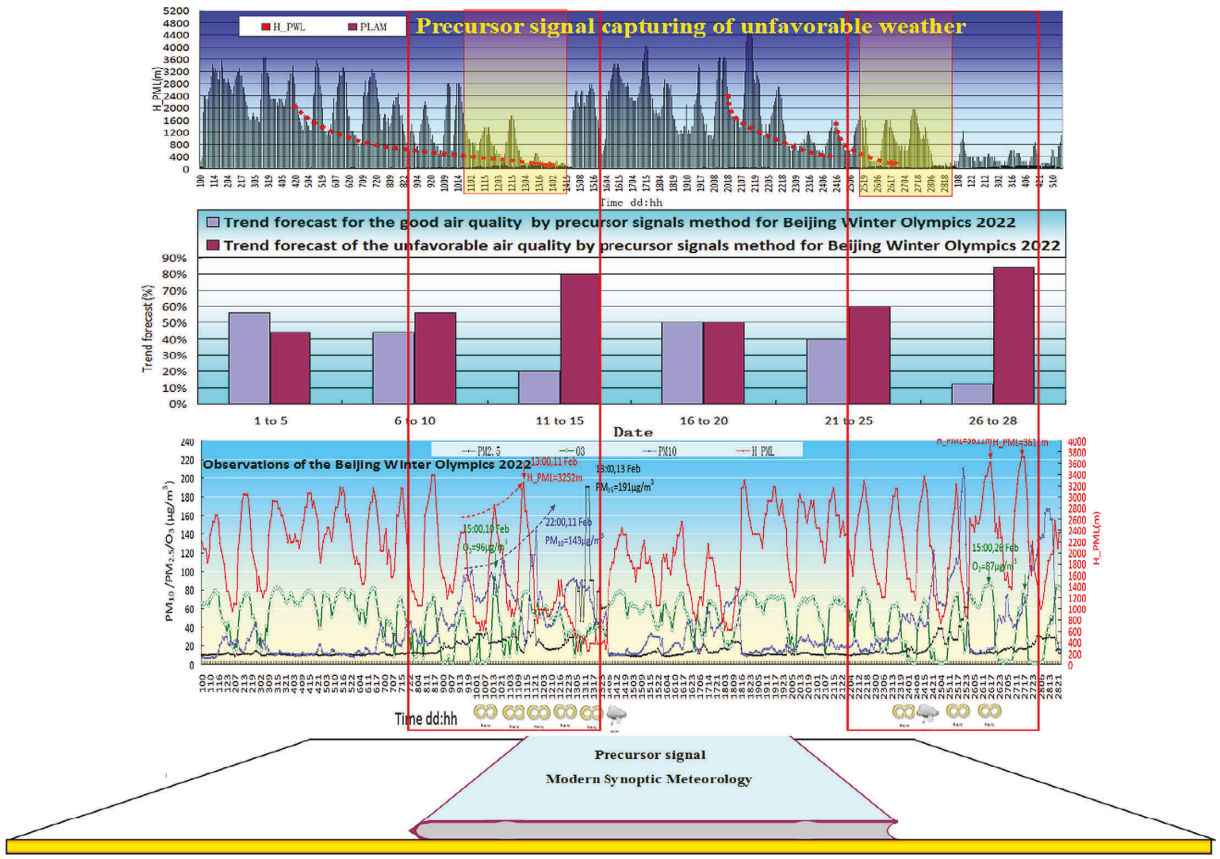

Figure 9: Comprehensive physical diagram of the precursor signal capturing for ultra-early high-resolution air quality weather prediction services.

transported to Beijing, and the predictive warning information of this precursor signal is very important.

3.3. Predicting the Trend of Precursor Signals of Unfavorable Meteorological Conditions during the Beijing Winter Olympics by the Historical Information of the Same Period (2017–2021)

3.3.1. Contribution to Emission Reduction during the Beijing Winter Olympics. Compared with the past 5–8 years, in the Beijing area, the pollutant emissions of heavy trucks have dropped by more than 90%, and 1 million diesel trucks below the national level III were previously eliminated. Air quality has improved significantly through emission reduction measures.

After the opening of the Winter Olympics, Beijing's air quality continued to be excellent. Monitoring data show that from February 4 to 17, the average concentration of $PM_{2.5}$ in Beijing was 24 $\mu g/m^3$, the $PM_{2.5}$ concentration in Beijing, Tianjin, and Hebei fell by more than 40% year-on-year, and the surrounding areas fell by more than 30% year-on-year. Especially on the day of the opening ceremony on February 4, the daily average concentration of $PM_{2.5}$ in Beijing was as low as 5 $\mu g/m^3$, and "Beijing Blue" became the default air quality at the Winter Olympic Games.

The Beijing Winter Olympics coincided with the traditional Chinese Spring Festival, for which fireworks control was already in place. During the Spring Festival, some enterprises stopped working, the level of social and economic activities dropped significantly, and the traffic flow was significantly reduced.

3.3.2. Comparative Analysis of Ultra-Early Prediction of High-Resolution (Hourly) Weather Changes with Observations for the Beijing Winter Olympics. Figure 8 shows the forecast analysis of the impact of meteorological conditions on air quality in the same period as the Beijing Winter Games for the past five years (2017 to 2021). It can be seen in Figure 8:

(1) According to the results of hourly precursor signal analysis in Beijing in February in the past five years, the probability of haze weather in Beijing from February 10 to15 is as high as 80%, while the probability of fine weather is less than 20%; that is, a forecast of unfavorable weather that would affect the Winter Olympics would be likely on February 10–15, 2022. Similarly, on February 26–29, the probability of adverse weather is as high as 83% or more, and the probability of fine weather is only 10%.

(2) As shown in Figure 8(b), the real-time observations of the Beijing Winter Olympics are very consistent with the forecast, with haze in Beijing from February 10 to 15, and similarly, heavy haze and thick fog from

February 24 to 28 (see the weather symbol at the bottom of Figure 8(b)).

(3) During the Beijing and Zhangjiakou Winter Olympics in February 2022, there were two times when the polluted weather process developed significantly and the air quality decreased meaningfully, which was consistent with the ultra-early forecast results based on the precursor signal capture theory method in this study. At 15:00 on February 10, the O_3 concentration was observed at 96 $\mu g/m^3$, and at 22:00 on February 11, PM_{10} soared to 143 $\mu g/m^3$ (indicated by the blue dotted line (see Figure 8(b)).

From the 10th to the 13th, the haze weather in Beijing lasted for 96 h, and there was drifting snow (see the weather symbol at the bottom of Figure 8(b), and in Figure 8(c), the note on the weather symbol of the ground weather map). The fog–haze in Beijing and Zhangjiakou and the hazy sky conditions affected the official schedule of the Winter Olympics. At that time, some projects, including the schedule of the women's U-pool ski race finals, had to be postponed for more than 48 h due to the haze and low VIS that could affect the health and landing skills of athletes.

Synthesizing the above, the theory and method for ultra-early high-resolution air quality weather prediction services are summarized as shown in Figure 9 through the capturing of precursor signals of adverse weather.

4. Conclusions

With the increasingly rapid development of economic globalization and the booming international economy, culture, and sports, including major events represented by Olympic competitions, the development of weather theory and technology brings many new challenges, and the existing traditional forecast programs for both research and operational purposes (both short- and long-term forecasts) require further technical updates. It is necessary to extend the forecast timeliness and add refinement to the forecast content, broaden the forecast domain, and meet the growth in public demand. One of the important growth areas for new developments in weather forecasting is how to predict transient signals of severe weather days or more months in advance and how to predict the evolution of transient signals, including down to hourly resolution, to provide a basis for the dispatch of large events. Research and development of atmospheric precursor signal prediction are of great importance. In this study, theoretical and methodological approaches for the influence of precursor signals on atmospheric processes are given for providing in the ultra-early stage of the unpredictable impact chain of transient unfavorable meteorological precursor signals. Through a more in-depth analysis of hourly information about several pollution processes over the last few years during the Beijing Winter Olympic Games (i.e., February), the precursor signal and observational facts of adverse meteorological conditions during the Winter Olympic Games are examined, as well as the theoretical and methodological approaches for the development of warning precursor signals. The results are as follows:

Assessment and analysis of historical weather and air quality in Beijing and Zhangjiakou concurrent with the Winter Olympic Games indicated air quality in Beijing and Zhangjiakou was affected by the same synoptic pattern synchronously. Research revealed that the precursor signal of adverse atmospheric processes can provide an ultra-early prediction for the frequent occurrence of low VIS fog–haze pollution, limited by space, starting with these typical cases of the Beijing Winter Olympics, including theoretical and methodological studies, as an initiation of enlightenment. The advantages of its research are that the data used in the study are real-time and included in the historical date, with high resolution and without the interference of emissions information (emission reduction control is more successful (zero growth of emissions)). It is beneficial to study the relative effects of meteorological conditions. We would suggest continuing to conduct in-depth research.

(1) The real-time observations of the Beijing Winter Olympics are consistent with the forecast and followed the precursor signal of the theoretical and methodological approaches used in this study. Beijing's persistent haze weather lasted from February 10 to 15, and fog–haze continued from February 24 to February 28, 2022.

(2) The first precursor signal in the atmosphere is the decreasing height of the mixing layer. In Beijing and Zhangjiakou, 2-3 days before the heavy pollution occurrence, a decrease in the mixing layer height was observed.

(3) The second atmospheric precursor signal is a signal of "negative $\longrightarrow$ positive" change in $\delta\Theta_e$. The atmospheric wet equivalent potential temperature change ($\delta\Theta_e$) appears as a "negative $\longrightarrow$ positive" signal, accompanied by a significant spike in atmospheric supersaturation (S), which is an important precursor indicator of heavy fog–haze pollution. Noting the key atmospheric precursor signal at the start of 2-3 days of pollution formation is conducive to accurate air quality forecasting services for the Winter Olympics Games.

(4) Hourly resolution $PLAM_{\longrightarrow obj}$ index can diagnose pollution transport in advance of the pollution precursor signal response in Beijing. During the same period of the Beijing Winter Olympics, the heavy haze pollution peaked at 472 $\mu g/m^3$ at 09:00 on February 13, 2021, during a record-breaking rare heavy pollution event. The $PLAM_{\longrightarrow obj}$ index provides quantitative precursor signal information about pollution transport to the Beijing region 40–60 h in advance.

(5) The analysis of universality in the microphysical condensation process of pollution precursor signals from seasonal and regional diagnostics indicates that the early detection of area features signaled by supersaturation can have almost universal application across parts of the North Hemisphere for identification, diagnosis, and prognosis of potential aerosol pollution.

5. Summary

It is necessary to extend the timeliness of forecasting while adding refinement to them has entered the focal science and interdisciplinary research area of "predictability" in modern weather forecasting. This study proposes the academic concept of establishing a captured precursor signal in modern synoptic meteorology. Based on this theoretical concept, and in view of the demand for day-by-day (including hourly resolution) weather forecasting services for typical cases of the 2022 Beijing Winter Olympics, the study gives the calculation and advanced capture methods of precursor hidden signals of air pollution mixed layer height changes, condensation, and supersaturation, as well as pollution transmission meteorological condition index, etc., and makes reasonable predictions. The study also gives the practicality of theories and methods in different regions (Vancouver, Canada, New York, USA).

Data Availability

The data used to support the findings of this study are available from the corresponding author upon request.

Additional Points

(1) Establish academic concepts to capture precursory signals in modern synoptic meteorology. (2) Months/years in advance to forecast hourly weather changes of the Beijing Winter Olympics. (3) Precursor signals of reduced height of mixed layer are coming 3–5 d before haze. (4) When the threshold of the supersaturated rising early signal is up to 6–7%, the haze will appear.

Conflicts of Interest

The authors declare that there are no conflicts of interest regarding the publication of this article.

Acknowledgments

The authors would like to thank Academician Zhang X.Y. for his valuable suggestions and comments. This study is supported by NSFC Major Project (42090031).

References

[1] T. Ondoh, "Investigation of precursory phenomena in the ionosphere, atmosphere and groundwater before large earthquakes of M > 6.5," *Advances in Space Research*, vol. 43, no. 2, pp. 214–223, 2009.

[2] D. W. King, E. S. Husebye, and R. A. W. Haddon, "Processing of seismic precursor data," *Physics of the Earth and Planetary Interiors*, vol. 12, no. 2-3, pp. 128–134, 1976.

[3] X. Y. Zhang, Y. Q. Wang, W. L. Lin et al., "Changes of atmospheric composition and optical properties over Beijing 2008 Olympic monitoring campaign," *Bulletin of the American Meteorological Society*, vol. 90, no. 11, pp. 1633–1652, 2009.

[4] X. Y. Zhang, X. D. Xu, and Y. H. Ding, *Effects of Changes in Meteorological Conditions from 2013 to 2017 on the Decline of PM2.5 Concentration in Key Areas of China*, Science China Earth Sciences, Berlin, Germany, 2019.

[5] J. T. Zhong, X. Zhang, K. Gui et al., "Reconstructing 6-hourly PM2.5 datasets from 1960 to 2020 in China," *Earth System Science Data*, vol. 14, no. 7, pp. 3197–3211, 2022.

[6] J. Z. Zhong, X. Zhang, Y. Dong et al., "Feedback effects of boundary-layer meteorological factors on cumulative explosive growth of PM2.5 during winter heavy pollution episodes in Beijing from 2013 to 2016," *Atmospheric Chemistry and Physics*, vol. 18, no. 1, pp. 247–258, 2018.

[7] J. Zhong, X. Zhang, Y. Wang et al., "Relative contributions of boundary-layer meteorological factors to the explosive growth of PM2.5 during the red-alert heavy pollution episodes in Beijing in December 2016," *Journal of Meteorological Research*, vol. 31, no. 5, pp. 809–819, 2017.

[8] RUSNEWS, *Sport-News*, RUSNEWS, Moscow, Russia, 2014.

[9] J. Zhu, "Challenges and countermeasures for air pollution prevention and control in the new era," *Low Carbon World*, vol. 4, pp. 12-13, 2018.

[10] B. J. Liu and Y. L. Zhang, "Comprehensive urban environmental governance and sustainable development," *Journal of China Environmental Management Cadre College*, vol. 16, no. 2, pp. 73–75, 2006.

[11] J. Z. Wang, Y Q. Yang, X. F. Jiang, D. Y. Wang, J. T. Zhong, and X. F. Wang, "Observational study of the PM2.5 and O3 superposition-composite pollution event during spring 2020 in Beijing associated with the water vapor conveyor belt in the Northern hemisphere," *Atmospheric Environment*, vol. 272, Article ID 118966, 2022.

[12] J. Z. Wang, S. L. Gong, X. Y. Zhang et al., "A parameterized method for air-quality diagnosis and its applications," *Advances in Meteorology*, vol. 2012, Article ID 238589, 10 pages, 2012.

[13] J. M. Wallace and P. V. Hobbs, *Atmosphere Science*, Elsevier Inc), Amsterdam, Netherlands, 2th edition, 2006.

[14] J. Liu, C. Lu, C. Li et al., "Ekman dynamics of the atmospheric boundary layer over the Antarctic Plateau in summer," *Chinese Science Bulletin*, vol. 59, no. 11, pp. 999–1005, 2014.

[15] Y. Li, W. Wang, J. Wang, X. Zhang, W. Lin, and Y. Yang, "Impact of air pollution control measures and weather conditions on asthma during the 2008 Summer Olympic games in Beijing," *International Journal of Biometeorology*, vol. 55, no. 4, pp. 547–554, 2011.

[16] Y. Ao, J. Li, Z. Li, S. Lyu, C. Jiang, and M. Wang, "Relation between the atmospheric boundary layer and impact factors under severe surface thermal conditions," *Advances in Meteorology*, vol. 2017, Article ID 8352461, 12 pages, 2017.

[17] C. Honoré, L. Rouil, R. Vautard et al., "Predictability of European air quality: assessment of 3 years of operational forecasts and analyses by the PREV'AIR system," *Journal of Geophysical Research*, vol. 113, no. D4, pp. D04301–D04623, 2008.

[18] B. Zhao, K. N. Liou, Y. Gu et al., "Enhanced PM2.5 pollution in China due to aerosol-cloud interactions," *Scientific Reports*, vol. 7, no. 1, p. 4453, 2017.

[19] X. Y. Zhang, Y. Q. Wang, T. Niu et al., "Atmospheric aerosol compositions in China: spatial/temporal variability, chemical signature, regional haze distribution and comparisons with global aerosols," *Atmospheric Chemistry and Physics*, vol. 12, no. 2, pp. 779–799, 2012.

[20] X. M. Hu, J. Huang, J. D. Fuentes, R. Forkel, and N. Zhang, "Advances in boundary-layer/air pollution meteorology," *Advances in Meteorology*, vol. 2016, Article ID 2825019, 2 pages, 2016.

[21] D. S. Yang, Y. B. Liu, and S. K. Liu, *Dynamics of Meteorology*, China Meteorological Press, Beijing, China, 2th edition, 1982.
[22] J. Holmboe, G. E. Forsythe, and W. Gustin, *Dynamic Meteorology*John Wiley and Sons, Inc, Hoboken, NJ, USA, 1952.
[23] M. A. Shapiro and J. T. Hastings, "Objective cross-section analyses by hermite polynomial interpolation on isentropic surfaces," *Journal of Applied Meteorology*, vol. 12, no. 5, pp. 753–762, 1973.
[24] T. W. Harrold, "Mechanisms influencing the distribution of precipitation within baroclinic disturbances," *Quarterly Journal of the Royal Meteorological Society*, vol. 99, no. 420, pp. 232–251, 1973.
[25] K. A. Browning, M. E. Hardman, T. W. Harrold, and C. W. Pardoe, "The structure of rainbands within a mid-latitude depression," *Quarterly Journal of the Royal Meteorological Society*, vol. 99, no. 420, pp. 215–231, 1973.
[26] S. T. Gao and Y. S. Zhou, "Analyses on warm and humid weather in summer in Beijing and its dynamical identification," *Science in China*, vol. 48, no. Suppl. II, pp. 128–137, 2005.
[27] X. J. Shen, J. Sun, X. Zhang, Y. Zhang, L. Zhang, and R. Fan, "Key features of new particle formation events at background sites in China and their influence on cloud condensation nuclei," *Frontiers of Environmental Science & Engineering*, vol. 10, no. 5, p. 1178, 2016.
[28] M. Kulmala, H. Vehkamaki, T. Petaja et al., "Formation and growth rates of ultrafine atmospheric particles: a review of observations," *Journal of Aerosol Science*, vol. 35, no. 2, pp. 143–176, 2004.
[29] J. Z. Wang, Y. Yang, X. Zhang et al., "On the influence of atmospheric super-saturation layer on China's heavy haze-fog events," *Atmospheric Environment*, vol. 171, pp. 261–271, 2017.
[30] I. Koren, Y. J. Kaufman, D. Rosenfeld, L. A. Remer, and Y. Rudich, "Aerosol invigoration and restructuring of Atlantic convective clouds," *Geophysical Research Letters*, vol. 32, no. 14, pp. 1–10, 2005.
[31] X. Y. Tang, Y. H. Zhang, and M. B. H. E. P. Shao, *Atmospheric Environmental Chemistry*, Higher Education Press, Beijing, China, 2006.
[32] C. Y. Lin, C. Zhao, and X. H. Liu, "Modeling of long-range transport of Southeast Asia biomass-burning aerosols to Taiwan and their radiative forcing over East Asia," *Tellus B: Chemical and Physical Meteorology*, vol. 66, 2014.
[33] T. Niu, J. Wang, Y. Yang, Y. Wang, and C. Chen, "A study on parameterization of the Beijing winter heavy haze events associated with height of pollution mixing layer," *Advances in Meteorology*, vol. 2017, Article ID 8971236, 11 pages, 2017.
[34] Y. Q. Yang, J. Z. Wang, X. Y. Zhang, H. Z. Che, and J. T. Zhong, "On the influence mechanism of meteorological conditions for the heavy pollution in Shenyang and the Song-Liao plain in January," *Journal of Meteorology and Environment*, vol. 4, pp. 15–26, 2018.
[35] J. Z. Wang, Y. Q. Wang, H. Liu et al., "Diagnostic identification of the impact of meteorological conditions on PM2.5 concentrations in Beijing," *Atmospheric Environment*, vol. 81, pp. 158–165, 2013.
[36] X. Y. Zhang, J. Z. Wang, Y. Q. Wang, H. L. Liu, J. Y. Sun, and Y. M. Zhang, "Changes in chemical components of aerosol particles in different haze regions in China from 2006 to 2013 and contribution of meteorological factors," *Atmospheric Chemistry and Physics*, vol. 15, no. 22, pp. 12935–12952, 2015.
[37] J. Z. Wang, Y. Yang, G. Deng et al., "Global view on China's foggy-haze associated with air-pollutant conveyor belts," *Science of the Total Environment*, vol. 693, pp. 133448–133514, 2019.
[38] X. Y. Zhang, J. Y. Sun, Y. Q. Wang et al., "Factors contributing to haze and fog in China (in Chinese)," *Chinese Science Bulletin*, vol. 58, pp. 1178–1187, 2013.
[39] W. Deying, Y. Yuanqin, L. Liangke, Z. Junting, W. Yaqiang, and W. Jizhi, "Formation mechanism of heavy haze-fog associated with the interactions between different scales of atmospheric processes in China," *Atmospheric Pollution Research*, vol. 12, no. 6, Article ID 101085, 2021.